Investigation of alumino-silicate glasses by coupling experiments and simulations: Part II - Radiation effects

J.-M. Delaye, A. Le Gac, S. Macaluso, F. Angeli, F. Lodesani, T. Charpentier, S. Peuget

Investigation of alumino-silicate glasses by coupling experiments and simulations: Part II - Radiation effects

J.-M. Delaye[1], A. Le Gac[1], S. Macaluso[1], F. Angeli[1], F. Lodesani[2], T. Charpentier[2], S. Peuget[1]

[1]CEA, DES, ISEC, DE2D, University of Montpellier, Marcoule, F-30207 Bagnols-sur-Cèze, France
[2]Université Paris-Saclay, CEA, CNRS, NIMBE, 91191 Gif-sur-Yvette Cedex, France

Key words:
Alumino-silicate glasses, Irradiation, Density, Molecular Dynamics, Raman Spectroscopy, NMR

Abstract

A set of SiO_2-Al_2O_3-Na_2O-CaO glasses with varying Si/Al and Na/Ca ratios was experimentally irradiated with Au^{4+} ions at 7.3MeV. Measurements by optical interferometry showed that depending on the glass composition, the density could increase or decrease. Overall, the higher the original quantity of non-bridging O, the greater the swelling observed.
In order to explain the origin of these observations, some of the experimentally studied glasses were simulated by classical molecular dynamics, and then subjected to a series of 4keV displacement cascades or quenched at different rates. Comparisons of the density changes and atomic-scale modifications have allowed the authors to propose a phenomenological density change model. There appears to have been a competition between two processes, with a first process where the vitreous structure "breathes", associated with the deposit of free volumes within the cascades that favours swelling. A second process is associated with changes in the local environments (creation of non-bridging O and of 3-coordinated O, creation of 5-coordinated Al, conversions between charge compensators and network modifiers) which act as brakes on the swelling. Depending on the relative dominance of these two processes, the glass may swell or contract.

1. Introduction

Vitreous matrixes, particularly alumino-borosilicate glasses, are widely used in the nuclear energy field to store radioactive wastes [1,2] and there have been numerous studies devoted to the effects of irradiation in this type of matrix [3,4,5]. In France, alumino-silicate glasses without boron oxide have also been considered for the containment of specific intermediate-level wastes [6]. Although alumino-silicate glasses also find many uses in other fields, like the optical or electronics industries, there have been very few studies focussing on the effects of irradiation on these matrices [7,8] whereas many studies related to their structures have been published [9,10].

Recently, damage caused by irradiation with 2.5MeV electrons was studied for a series of glasses composed of SiO_2, Al_2O_3, Na_2O, and CaO in varying quantities [11]. Different types of electronic defects were brought to light using EPR (defects like OHC, Al, E' centres), with maximum concentrations for an irradiation dose of 1GGy. The defect concentrations decreased for higher doses.

Here, the authors follow up on the previous study and focus on investigating the effects of a deposit of nuclear energy on glasses with the same compositions as those examined before.

To study the damage caused by a deposit of nuclear energy, irradiation experiments using external heavy ion beams were coupled with classical molecular dynamics simulations. This simulation method is in fact very interesting, and it is commonly used to investigate structural changes at the atomic scale and to correlate these with macroscopic property changes [12,13,14,15,16].
For the alumino-silicate glass simulations, several potentials are available in the literature [17,18,19,20,21,22]. The authors checked in the first part of this two-part article the relevance of the potential proposed by Deng et al. [**Erreur ! Signet non défini.**] to accurately reproduce the structures of alumino silicate glasses [23,24]. These potentials were used here to simulate series of ballistic collisions within the SiO_2-Al_2O_3-Na_2O-CaO glasses. In the first part of this two-part article, the structures of these vitreous compositions, characterized experimentally and simulated by classical molecular dynamics, are described in detail.

Following experimental irradiation by heavy ions and depending on the glass composition, the density could increase or decrease. An even greater swelling could be measured in peralkaline glasses when the quantity of non-bridging oxygens rose. However in peraluminous glasses, in which all the charge compensators were mobilized to compensate the AlO_4 tetrahedra, the density increased, i.e. irradiation led to glass shrinkage.
In order to be able to propose a phenomenological model explaining the origin of density changes depending on the glass composition, atomistic modelling was used.

This article is organized as follows. The experimental and numerical methods are described in paragraph 2. Then the glass structure modifications following irradiation with heavy ions are described in paragraphs 3.1 and 3.2, while the macroscopic property modifications are given in paragraph 3.3. The results from classical molecular dynamics simulations are detailed in paragraph 3.4. Finally, in the discussion (paragraph 4), the authors propose a phenomenological model to explain the origin of glass swelling or shrinkage under irradiation.

2. Methods

2.1 Glass fabrication and experimental methods

The method used to fabricate the glasses was described in the first article of this two-part study. Table 1 shows all the compositions prepared experimentally. The glass compositions were measured by EDS. The same names are used as in the first part of this article.

Series 1	**SiO_2**	**Na_2O**	**Al_2O_3**	**CaO**
Na	65.6	27.1	7.4	0.0
Na/Ca 1.4	59.9	19.8	6.6	13.7
Na/Ca 0.3	58.0	9.1	6.5	26.4
Ca	55.6	0.0	7.3	35.5

Series 2	**SiO_2**	**Na_2O**	**Al_2O_3**	**CaO**
NBO1	66.0	19.1	2.8	12.1
NBO2	62.6	19.5	5.4	12.5
Na/Ca 1.4	59.9	19.8	6.6	13.7

NBO4	57.0	20.4	8.0	14.6
NBO5	52.1	22.0	10.6	15.3

Series 3	**SiO_2**	**Na_2O**	**Al_2O_3**	**CaO**
Na/Ca 1.4	59.9	19.8	6.6	13.7
Si/Al 5.4	55.6	20.3	10.3	13.9
Si/Al 2.4	48.7	18.0	20.7	12.6
Si/Al 1.6	43.9	16.5	28.3	11.3
Si/Al 1.4	41.7	14.4	29.8	13.8
Si/Al 1.3	41.4	15.3	31.8	11.3

Table 1: Series of glasses prepared experimentally. Compositions in molar percentages are measured by EDS.

The characteristics of the measurements by NMR and Raman spectroscopy were explained in the first part of this two-part article, and will not be repeated here.

2.2 Experimental irradiations

The 13 glasses in the three series were irradiated with 7.3MeV Au^{4+} ions on the JANNuS platform (CEA Saclay), at a flux of 1.5 10^{10} ions/cm^2/s in order to reach a total fluence of 1x10^{14} ions/cm^2. The ion incidence angle was 15°, which is equivalent to 7MeV ions penetrating the surface perpendicularly. The energies deposited in electronic and nuclear form were respectively 0.24GGy and 70MGy. Although the deposit of electronic energy was higher than that of nuclear energy, the ballistic effects associated with the deposit of nuclear energy dominate the consequences for the glass structure, as the literature has shown this form of energy to be 100 times more efficient in generating structural damage [25,26]. This nuclear energy dose is sufficient to reach saturation effect.

The penetration depth of the Au^{4+} ions, estimated with the TRIM code, is approximately 2µm (Figure 1).

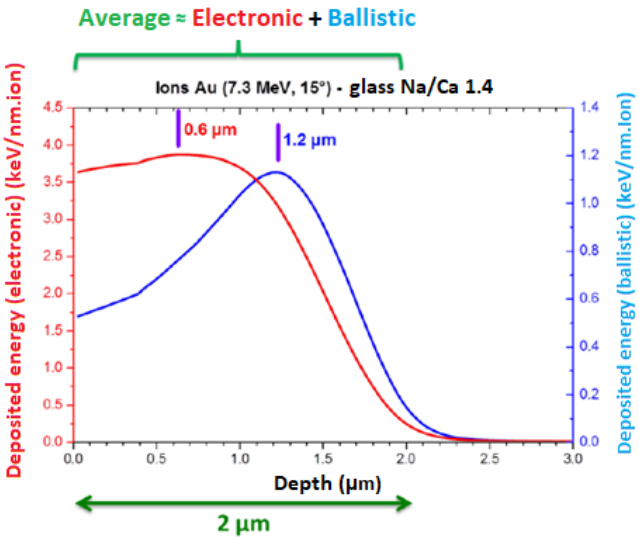

Figure 1: TRIM simulation of the penetration of 7.3MeV Au ions into the Na/Ca 1.4 glass (incidence angle of 15°). The deposits of electronic and nuclear energy are indicated in red and blue.

The irradiated samples were 4mm square and 500µm thick, optically polished on one side and on the edges. Aluminium masks had been placed on the samples to block part of the beam and form a step between the irradiated and non-irradiated parts. Measurement of the step height by optical interferometry enabled the density variations to be found, knowing the ion penetration depth.

Two glasses (Na/Ca 1.4 and Na/Ca 0.3) were irradiated in the form of powders with a granulometry of less than 2µm. Mono grain deposits were prepared so that the Au ions went completely through each grain (7MeV Au^{3+} ions were used, on the ARAMIS accelerator (GANIL – Caen – France)). The irradiation fluence was $1x10^{14}$ ions/cm^2.

2.3 Simulations of the irradiation effects

The compositions of the simulated glasses, in molar percentages, are listed in Table 2 (note that because of calculation times, only some of the experimental glasses were irradiated by displacement cascade series). These compositions were chosen to cover a wide interval and to have both glasses that swelled under irradiation and glasses that contracted [27].

For the classical molecular dynamics simulations, each glass was contained within a cubic simulation cell of 60000 atoms. Buckingham-type potentials were used. For two atoms i and j separated by a distance r_{ij}, the following interaction potential was applied:

$$\Phi(r_{ij}) = \frac{q_i q_j}{r_{ij}} + A_{ij} exp\left(-\frac{r_{ij}}{\rho_{ij}}\right) - \frac{C_{ij}}{r_{ij}^6} \qquad (1)$$

The adjustable parameters and the charges were taken from the work of Deng et al. [**Erreur ! Signet non défini.**]. The charges were fixed. Coulombic interactions were calculated according to the Ewald formalism with a precision of 10^{-5} [28,29]. The cut-off for the other pair terms was set at 10Å.

In the first part of this two-part article, published, we showed that these potentials enable the reproduction of a large number of the experimental glass structural characteristics.
The DLPOLY code [30] was used for the glass preparation and to calculate the displacement cascades.

The initial structures were prepared as follows. Firstly, a random departure configuration was constructed imposing a minimum distance between two atoms, to avoid overly intense interactions in the first steps. Next, a liquid was equilibrated at 4000K for 10^5 steps of 1fs. This liquid was then quenched at a rate of 10^{12}K/s down to 300K, lowering the temperature in 20K steps. The duration of each step was set at 2 10^4 steps of 1fs to ensure a quenching rate of 10^{12}K/s. A last relaxation for 5 10^3 steps of 1fs at 300K enabled the preparation of the initial structure to be finalized. The volume remained constant during all the fabrication stages, and was set in order to reproduce the experimental density of the glasses (Table 2).

Glass	**SiO_2**	**Al_2O_3**	**Na_2O**	**CaO**	**Experimental density**	**Length of the diagonal**
Na	59.9	6.6	19.8	13.7	2.592	161,08

Na/Ca 0.3	57.9	6.5	9.2	26.4	2.669	161,22
Ca	56.5	7.4	-	36.1	2.79	160,18
Si/Al 5.4	55.6	10.3	20.3	13.8	2.591	161,13
Si/Al 2.4	48.7	20.7	18	12.6	2.569	161,74
Si/Al 1.3	41.4	31.9	15.3	11.4	2.606	160,45

Table 2: Molar compositions of the simulated glasses, experimental densities, and main diagonal of the simulation boxes (in Å).

For the displacement cascade simulations, first of all 8 Si atoms were given the mass of a U atom and thus to have heavy projectiles suitable for initiating displacement cascades. These projectiles were accelerated one after the other to accumulate high doses of nuclear energy.

For the displacement cascade calculations, ZBL-type potentials were added at a short distance [31]. They were coupled to Buckingham-type potentials by polynomial connections, which ensured the energy, force, and force derivative continuity.

To accumulate the displacement cascades, 120 projectiles were successively accelerated at an energy of 4keV in a direction corresponding to one of the main diagonals of the simulation box. A translation was applied before each cascade in order to position the projectile towards one of the extremities of the main diagonal and the same translation (taking into account periodic conditions) was applied to the other atoms to avoid modifying the structure. The simulation box was thus subjected to an increasing deposit of nuclear energy and a new stationary state was rapidly reached, as shall be seen below.

During the displacement cascades, the external layer of the simulation box was maintained at 293K for a thickness of 2Å to remove the surplus of thermal agitation created by the initial acceleration of the projectile. To achieve this, the speeds of the atoms in the external layer were thermalized at 293K.

Checks were made to ensure that the trajectories followed by the projectiles remained well within the confines of the simulation box and that their dynamics were not disturbed by the temperature controls on the external layers. Table 2 gives the lengths of the main diagonals for each box. The TRIM code made it possible to estimate the trajectory length for a 4keV projectile with a mass equal to that of U, when the density and composition of a glass are known. A maximum length of 74.55Å was obtained for the Si/Al 2.4 glass, which remains significantly less than the lengths of the main diagonals.

The following method was applied to measure the swelling or shrinkage under irradiation. As the simulation box volumes were fixed in order to reproduce the experimental densities, a first reference calculation was made by relaxing the initial structure in the NPT ensemble (for 20000 steps of 1fs) then in the NVE ensemble (for 5000 steps of 1fs) to measure the initial equilibrium density. A second reference calculation was done by applying the same relaxation in the NPT and NVE ensembles to the vitreous structure that had accumulated 120 displacement cascades. The equilibrium volume of the irradiated glass was thus determined. The difference between the initial and final reference volumes enabled an estimation of the density variation under irradiation.

3. Results

3.1 Modifications to the local environment of the Al

^{27}Al NMR MAS and MQMAS results recorded for the irradiated powders pointed to a modification in the spectra after irradiation (Figure 2).
Whereas all the Al had been observed to be 4-coordinated in the pristine glasses (see the first part of this two-part article), 5-coordinated Al formed after irradiation in a proportion estimated to be around 3%, slightly higher for the Na/Ca 0.3 glass than for the Na/Ca 1.4 (Figure 3). Nevertheless, most of the Al remained 4-coordinated. Note that there were traces of 6-coordinated Al (less than 1%) in the Na/Ca 0.3 glass.

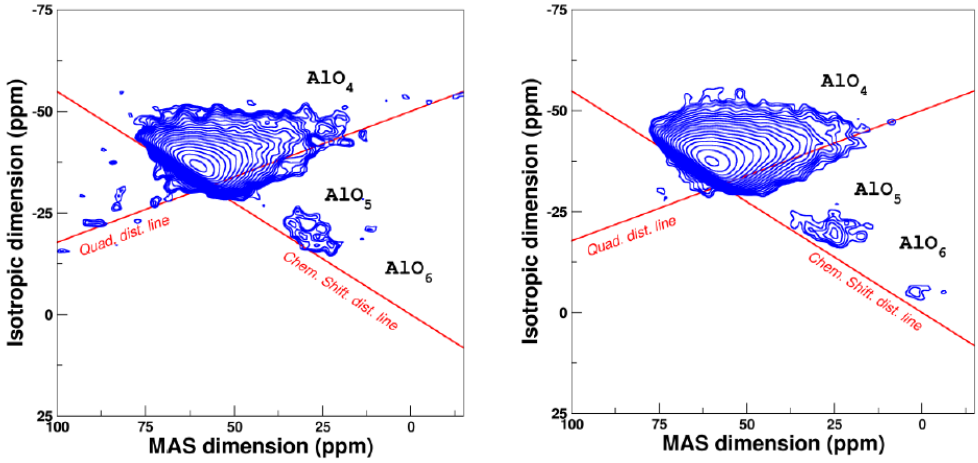

Figure 2: MQMAS spectra for ^{27}Al recorded on the Na/Ca 1.4 (left) and Na/Ca 0.3 (right) glass powders irradiated by 7MeV Au^{3+} ions.

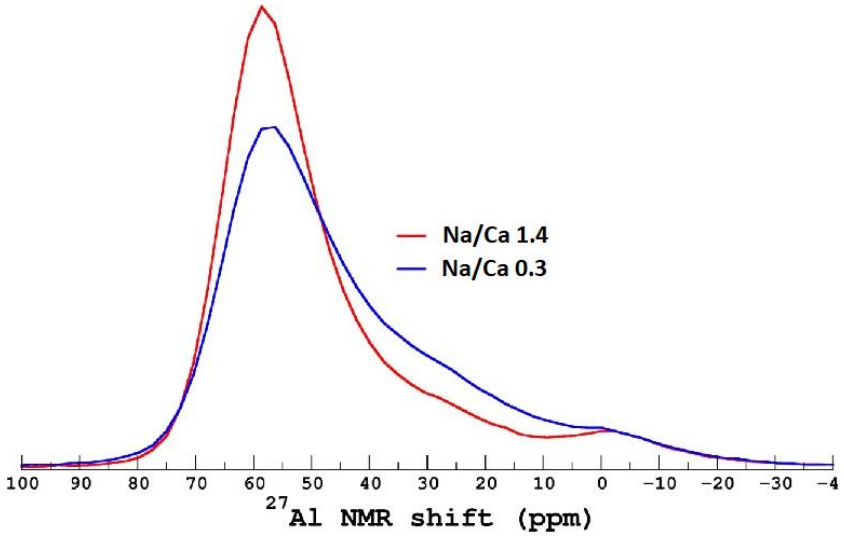

Figure 3: Comparison between the ^{27}Al NMR spectra for the Na/Ca 1.4 (red) and Na/Ca 0.3 (blue) glasses irradiated by 7MeV Au^{3+} ions.

The broadening of the NMR MQMAS spectra for ^{27}Al, which can be seen along the quadripolar distribution line ("Quad. Dist. Line"), reflects an increase in the disorder of the Al environments, which could be explained by a growing number of Ca as charge compensators replacing the Na. However, this result should be treated with caution, as a Na depletion was

observed on the surface of the samples, and these observations may well come from surface effects.

3.2 Structural modifications at medium distance

Micro-Raman spectra were recorded from the irradiated parts of the glasses at a depth of approximately 1µm below the surface.
There were various spectrum modifications depending on the composition involved, which did not simplify the establishment of general rules. In Figures 4-7 we only show the spectra which will be discussed in more detail in this paragraph. The other available Raman spectra acquired from the pristine and irradiated glasses are given in the Supplementary Information.

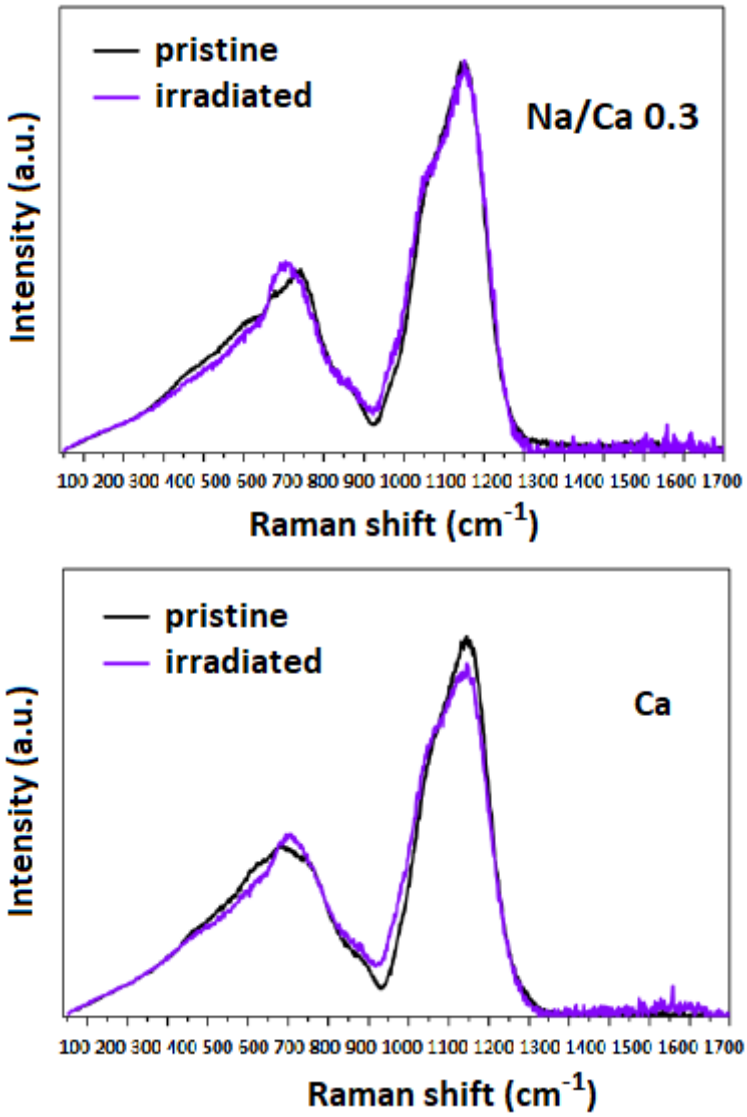

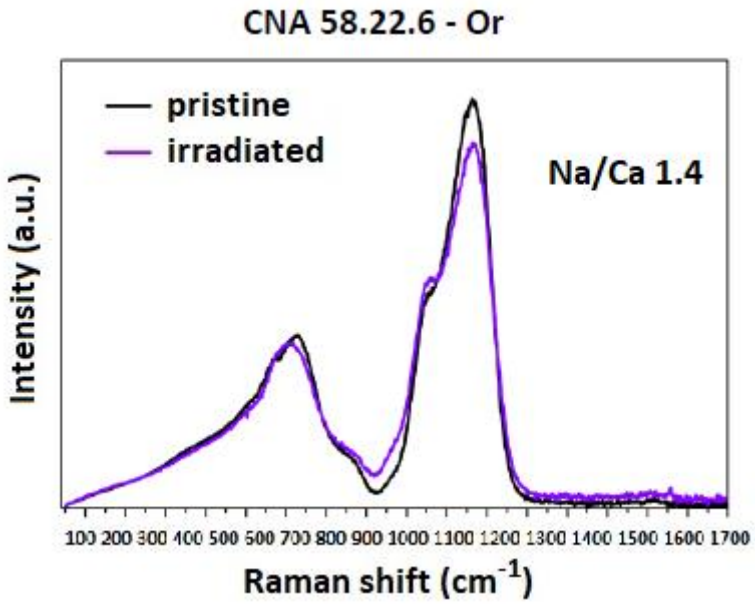

Figure 4: Raman spectra for the pristine and irradiated Na/Ca0.3, Ca, and Na/Ca 1.4 glasses. The intensities are given in arbitrary units and normalized at the spectra surfaces.

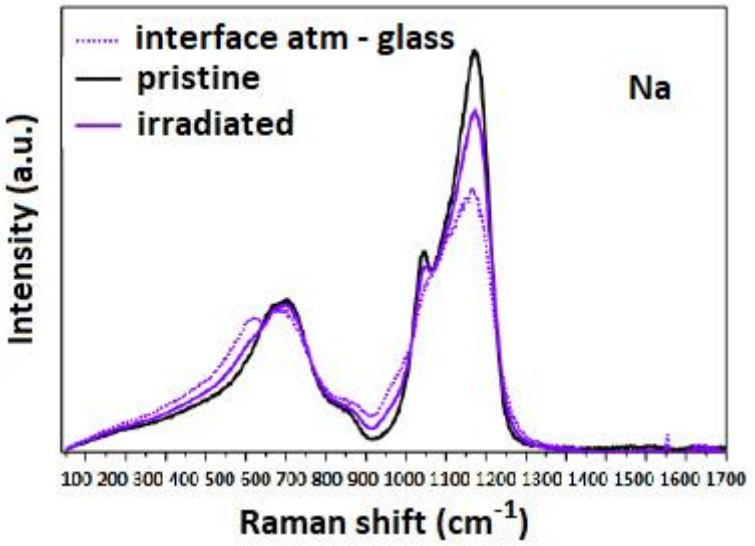

Figure 5: Raman spectra for pristine and irradiated Na glass. The figure also shows the spectrum acquired at the interface between the atmosphere and the glass. The intensities are given in arbitrary units and normalized at the spectra surfaces.

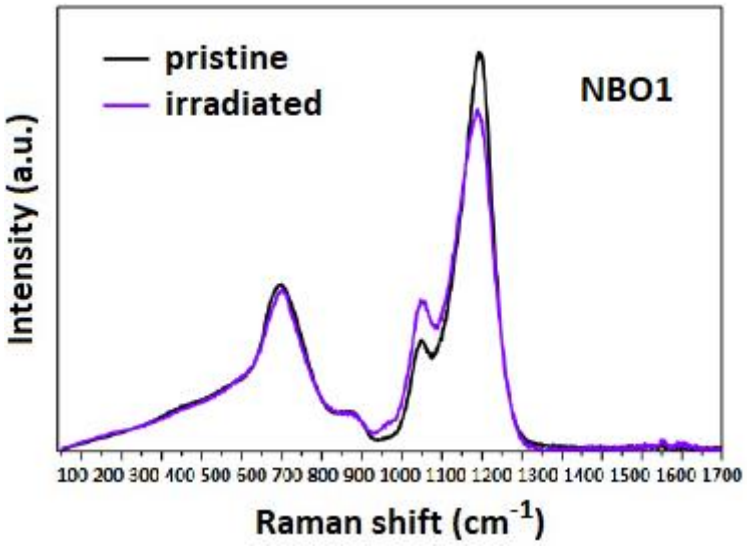

Figure 6: Raman spectra for pristine and irradiated NBO1 glass. The intensities are given in arbitrary units and normalized at the spectra surfaces

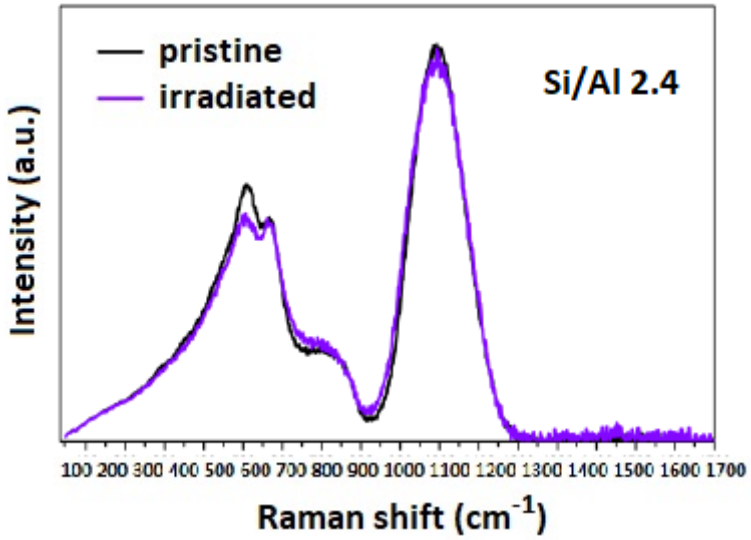

Figure 7: Raman spectra for pristine and irradiated Si/Al 2.4 glass. The intensities are given in arbitrary units and normalized at the spectra surfaces

Overall, and based on all the Raman spectra, it appears that for Series 1 the structural changes decrease with the Na/Ca ratio, which seems to contradict the NMR (which saw more changes in the Na/Ca 0.3 glass than in the Na/Ca 1.4). In the Series 2 and 3, the structural changes decreased when the Al_2O_3/SiO_2 ratio or the Al_2O_3 content increased.

Certain particularly notable results are indicated below:

- In two Series 1 glasses (Na/Ca 0.3 and Ca), the intensity of the contribution at 510cm^{-1} dropped considerably whereas the line at 600cm^{-1} increased in intensity and decreased in width. A rupture of the Al-O-Al bonds and a reduction in the distribution of the Si-O-Si and Si-O-Al angles are suspected.

- Very slight movements of the Q_n line (800-1200cm^{-1}) towards low frequencies could also be observed in the Na/Ca 0.3 and Ca glasses after irradiation, which might be due

to the presence of a few more aluminium atoms on average in the vicinity of the Q_n units [32,33]. In the same region, the irradiated Na/Ca 1.4 glass (Figure 4) presented a shoulder visible towards 875cm^{-1} which could be due to bond vibrations in Q_1 units [34], as well as a slight inversion of the Q_2 and Q_3 contributions with, in particular, a decrease in the intensity of the line at 1060 cm^{-1} corresponding to the Q_3-(Na, Ca).

- The Na glass showed atypical behaviour (Figure 5). For this sample, the contribution at 510cm^{-1}, not present in the pristine glass, became visible and the Q_n line decreased in intensity while widening overall. The considerable modification to the surface of this glass following a migration of the Na atoms over a depth of about 2.7µm, the same order of magnitude as the irradiation depth, makes it difficult to separate surface effects from irradiation effects for this glass.

- In the Series 2 glasses, only the Q_n line was impacted, in particular for the NBO1 glass (Figure 6) which presented a clear inversion of the Q^2 and Q^3 populations, possibly coming from a shift in the equilibrium $Q^3 = Q^2 + Q^4$ towards the right. For the other Series 2 glasses (spectra shown in the Supplementary Information), only slight overall decreases of the Q_n line were observed.

- For the Series 3 glasses, a decrease in the intensity of the line at 510cm^{-1} (Al-O-Al) was seen as from the Si/Al 2.4 glass (Figure 7), which corresponds to a drop in the number of Al-O-Al.

3.3 Modifications to the macroscopic properties

Macroscopically, the glasses showed either swelling or a contraction after irradiation by Au^{4+} ions. Table 3 lists the values for the changes in density of the different glasses.

Series 1	**SiO_2**	**Na_2O**	**Al_2O_3**	**CaO**	**ZrO_2**	**ΔV/V**	**%NBO**
Na	65.6	27.1	7.4	0.0	0.0	0.78%	21.8
Na/Ca 1.4	59.9	19.8	6.6	13.7	0.0	0.83%	31.0
Na/Ca 0.3	58.0	9.1	6.5	26.4	0.0	0.55%	33.9
Ca	55.6	0.0	7.3	35.5	1.6	0.68%	31.1

Series 2	**SiO_2**	**Na_2O**	**Al_2O_3**	**CaO**	**ZrO_2**	**ΔV/V**	**%NBO**
NBO1	66.0	19.1	2.8	12.1	0.0	0.74%	33.0
NBO2	62.6	19.5	5.4	12.5	0.0	0.74%	30.7
Na/Ca 1.4	59.9	19.8	6.6	13.7	0.0	0.83%	31.0
NBO4	57.0	20.4	8.0	14.6	0.0	0.88%	31.2
NBO5	52.1	22.0	10.6	15.3	0.0	1.00%	30.9

Series 3	**SiO_2**	**Na_2O**	**Al_2O_3**	**CaO**	**ZrO_2**	**ΔV/V**	**%NBO**
Na/Ca 1.4	59.9	19.8	6.6	13.7	0.0	0.83%	31.0
Si/Al 5.4	55.6	20.3	10.3	13.9	0.0	0.62%	27.1
Si/Al 2.4	48.7	18.0	20.7	12.6	0.1	-0.53%	10.3
Si/Al 1.6	43.9	16.5	28.3	11.3	0.1	-1.53%	0.0
Si/Al 1.4	41.7	14.4	29.8	13.8	0.2	-1.59%	0.0
Si/Al 1.3	41.4	15.3	31.8	11.3	0.2	-1.80%	0.0

Table 3: Variations in volume (ΔV/V) after Series 1, 2 and 3 glasses underwent irradiation by Au^{4+} ions. Positive values correspond to a swelling, and negative values to a contraction. The molar percentages of non-bridging O are indicated for each glass.

These magnitudes were measured considering the height of the step formed during the irradiation (measurement by optical interferometry) and on the basis of the ion penetration depth estimated by the SRIM code. But the TOF-SIMS measurements carried out on two glasses (Na and Na/Ca 1.4) had shown that this code tended to significantly underestimate the ion penetration depth, which added a bias to the density change calculations without however raising doubts as to its nature (swelling or shrinkage). This data can be found in the Supplementary Information.

As the Au ion penetration profiles had not been measured by TOF-SIMS for all the glasses, it was not possible to correct all the values, and therefore to remain coherent, the values estimated based on the penetration depths estimated by SRIM were used.
The swelling amplitudes clearly correlate to the quantity of non-bridging O, as shown in Figure 8. The higher this amount, the greater the swelling. On the contrary, when there was only a small amount of non-bridging O, the glasses contracted.

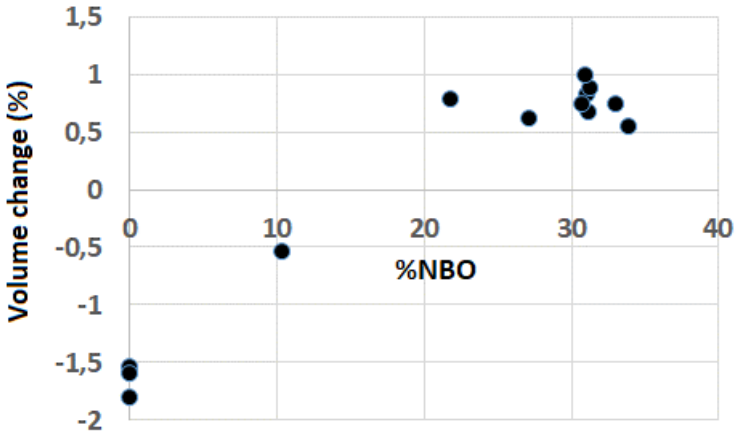

Figure 8: Change in volume (%) after irradiation as a function of the quantity of non-bridging O.

3.4 Simulation results

3.4.1 Reaching a new stationary state

The glasses listed in Table 2 were each subjected to a series of 120 4keV displacement cascades, according to the protocol detailed in the Methodology section. Whatever the composition, a new stationary state was reached systematically, as shown by the stabilisation of the internal pressure (Figure 9).
The evolution of the internal pressure (ΔP) depending on the number of cascades (n) follows a Marples-type law [35]:

$$\Delta P(n) = A[1 - exp(-B * n)] \qquad (3)$$

Parameter A corresponds to the variation in pressure at saturation and the magnitude B*V, with V being the initial volume of the simulation box, is the average elemental volume disturbed by an individual cascade. The values for these average volumes are given in Table 4.

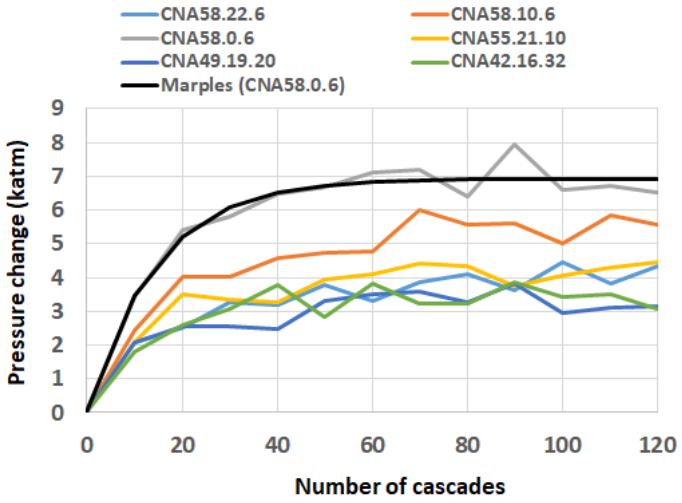

Figure 9: Evolution of the pressure (in katm) with the number of 4keV cascades in the different glasses. The Marples model is only shown for the Ca glass, in order to avoid overloading the figure.

Na/Ca 1.4	Na/Ca 0.3	Ca	Si/Al 5.4	Si/Al 2.4	Si/Al 1.3
43,4	41.8	55.1	53.8	60.9	59.8

Table 4: Average volume (in nm^3) disturbed by an individual 4keV cascade in the different glasses.

This average volume decreased when the Si/Al ratio increased (Figure 10), which shows that the replacement of Si by Al limited the volume affected by an elemental cascade. This can be interpreted by the fact that the cohesion forces that connect the Si to the network are stronger than those which connect the Al, as the charge of a Si is stronger than that of an Al.

The fact that the pressure variations with the number of cascades follow a Marples-type law means that locally irradiating the material once is enough to reach the stationary state.

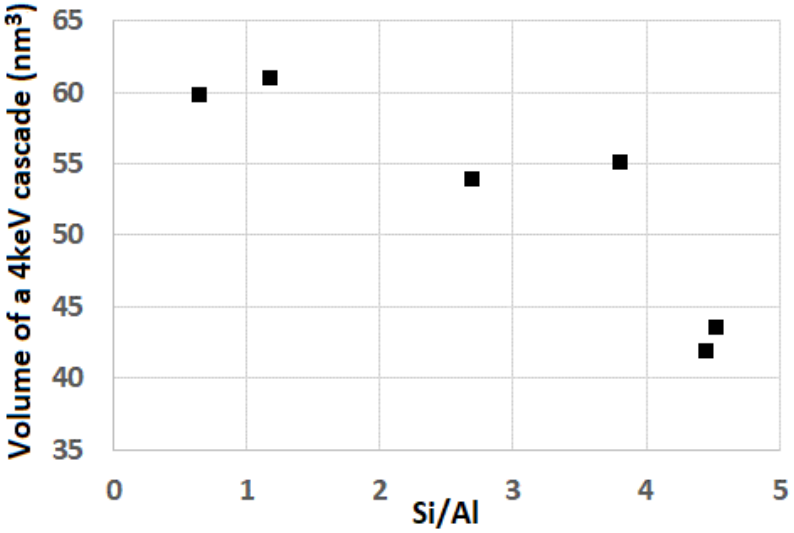

Figure 10: Average elemental volume (in nm^3) of a 4keV cascade as a function of the Si/Al ratio.

Figure 11 shows the evolution of the 2-coordinated Oxygen content (i.e. bridging oxygens) as a function of the number of cascades in the different glasses.

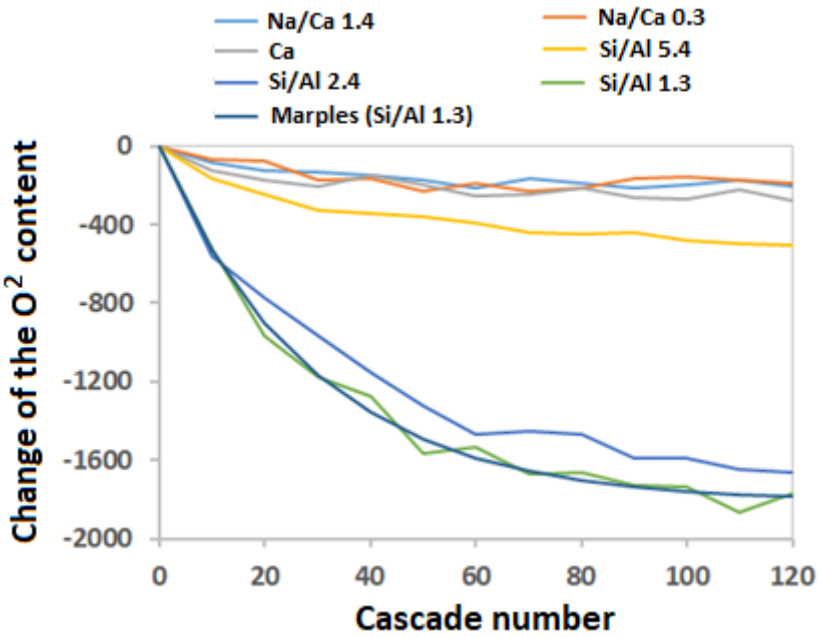

Figure 11: Variation in the number of bridging oxygens as a function of the number of 4keV cascades in the different glasses. The adjustment by a Marples-type model is shown for the Si/Al 1.3 glass.

Once again, the evolutions follow Marples-type laws to reach saturation for the strongest doses. To avoid overloading Figure 11, the Marples model adjustment is only shown for the Si/Al 1.3 glass.

The energy necessary to reach saturation both for the pressure and for the bridging oxygen content is around 60 cascades, i.e. an energy of approximately 4eV/atom, a value of the same order of magnitude as that measured in simple borosilicate glasses [36].

3.4.2 Changes in density and structural modifications

The configurations which had accumulated 120 4keV displacement cascades were relaxed in the NPT then NVE ensembles, according to the protocol previously described, to determine their new equilibrium densities (Table 5). Comparison with the initial reference densities enabled the determination of the density changes caused by the irradiation. The densities before and after irradiation are also listed in Table 5.

Glass	Initial density	Final density	Density change
Na/Ca 1.4	2.59	2.56	-0.96%
Na/Ca 0.3	2.67	2.64	-1.25%
Ca	2.76	2.73	-1.23%
Si/Al 5.4	2.59	2.57	-0.86%

Si/Al 2.4	2.58	2.56	-0.61%
Si/Al 1.3	2.62	2.61	-0.54%

Table 5: Initial and final densities, and density change caused by the series of 4keV displacement cascades.

The simulated density variations are drawn as a function of the experimental values in Figure 12. Although the simulation results lead to a systematic swelling for all the glasses, correlation with the experiment was not lost. The greater the experimental swelling, the greater the simulation swelling. Furthermore, the higher the experimental densification, the weaker the simulated swelling. The hierarchy of density changes thus remains relatively well reproduced even if no shrinkage is observed here.

The absence of densification during the simulations is discussed in the following sections. We sought to correlate the density changes with the changes in structural characteristics.

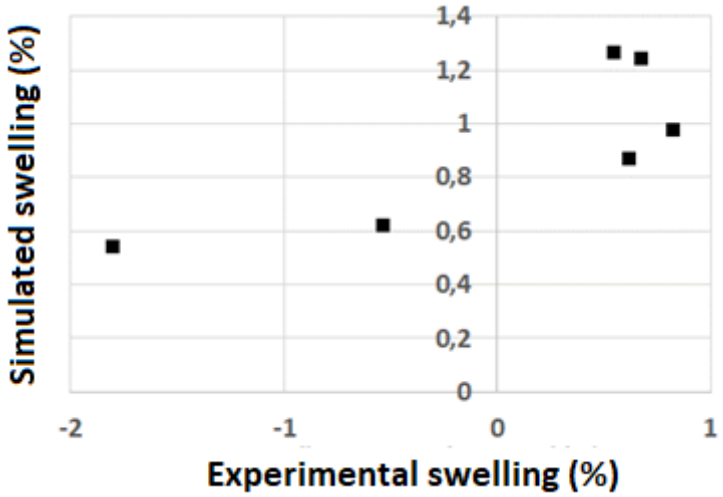

Figure 12: Simulated swelling as a function of the experimental swelling.

Table 6 contains the variations in the quantities of non-bridging oxygens (NBO), of 3-coordinated oxygens (O^3), and of 5-coordinated Si and Al (Si^5 and Al^5) following irradiations. Here, the initial and final structures after relaxations in the NPT and NVE ensembles were considered.

Glass	**NBO**	**O^3**	**Si^5**	**Al^5**
Na/Ca 1.4	49	161	3	17
Na/Ca 0.3	31	161	13	4
Ca	95	191	16	-10
Si/Al 5.4	203	289	2	32
Si/Al 2.4	819	852	1	67
Si/Al 1.3	834	927	3	159

Table 6: Variations in the quantities of NBO, O^3, and of 5-coordinated Si and Al after irradiation.

The variations in the number of 5-coordinated Si remained weak and will not be discussed here. On the other hand, there appear to be clear correlations between the swelling and the variations in the quantities of NBO, of O^3, and of Al^5 (Figure 13).

The swelling is all the weaker when the variations in the quantities of NBO, O^3, and Al^5 are high. Another interesting point should be noted. The variations in the quantities of NBO and of O^3 under irradiation are correlated almost linearly, as shown in Figure 14 (a linear adjustment gives a slope of 0.94, close to 1). The formation mechanisms of the NBO and the O^3 are therefore strongly correlated, and these two entities form conjointly.

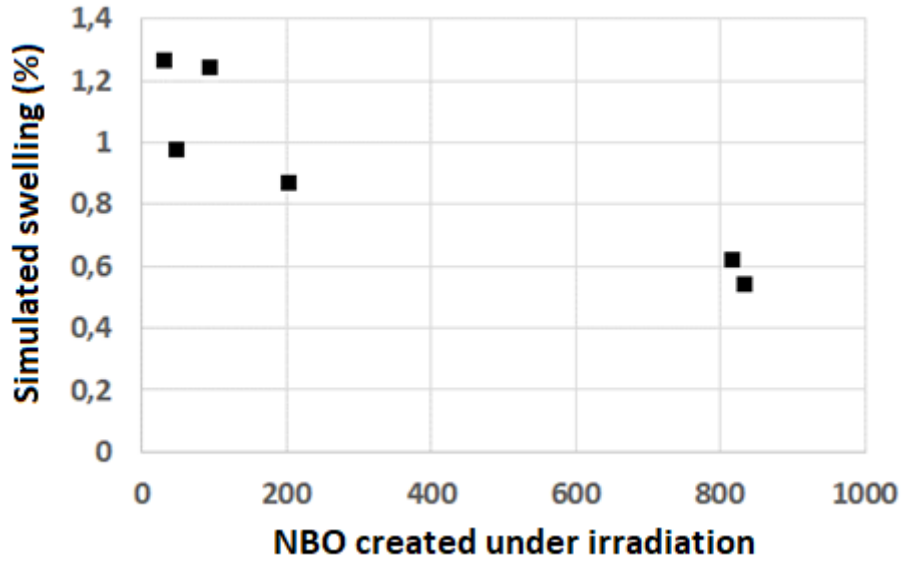

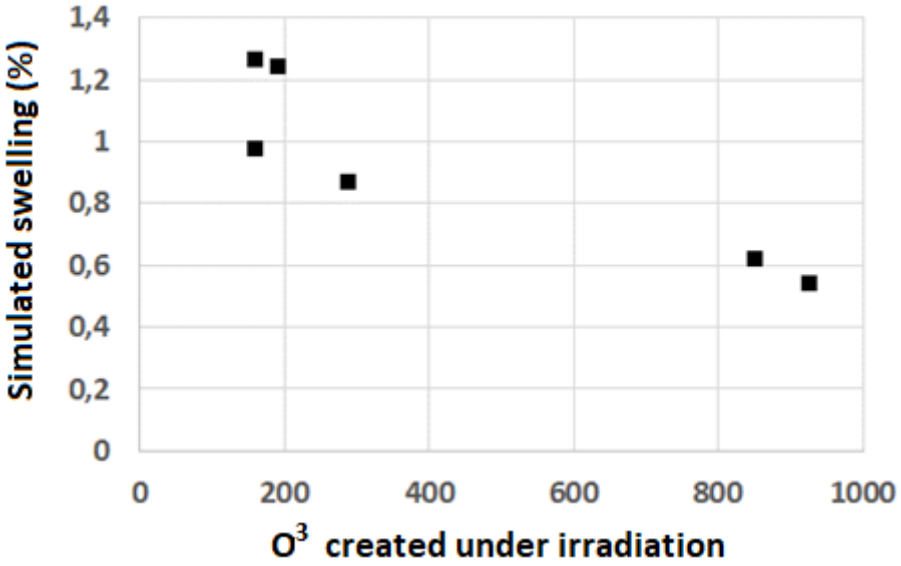

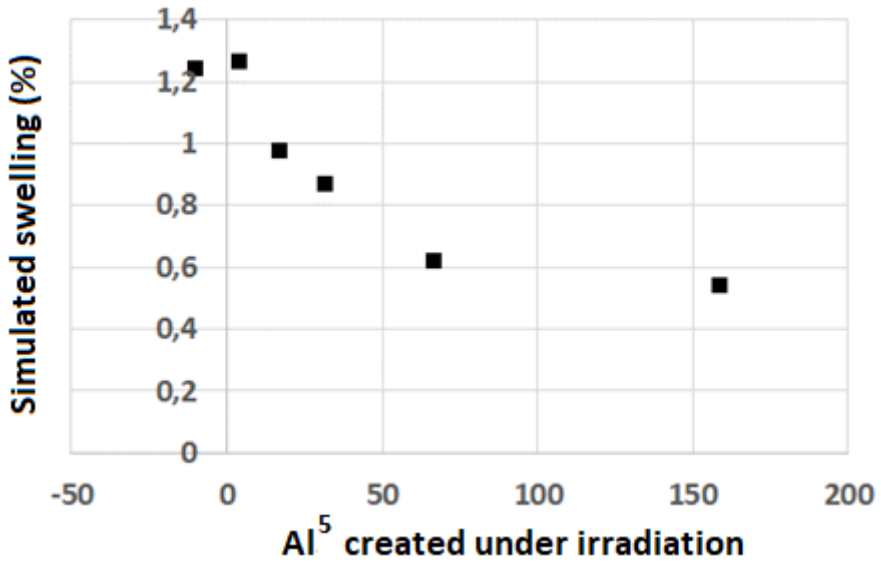

Figure 13: Correlations between swelling and variations in the quantities of NBO, O^3, and Al^5.

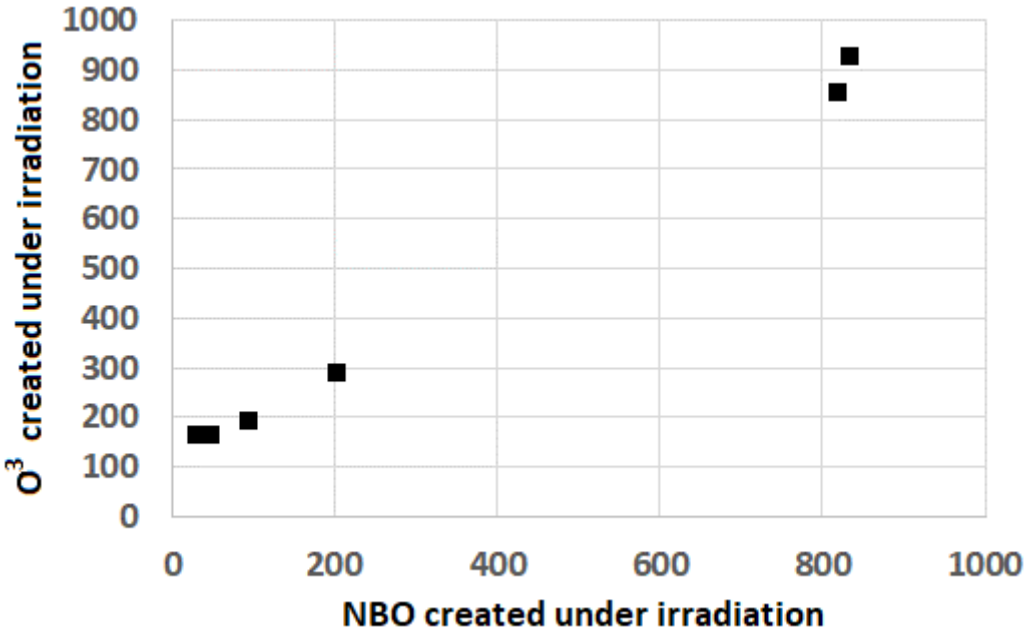

Figure 14: Variation in the quantity of O^3 as a function of the variation in the quantity of NBO formed under irradiation.

It therefore appears that two mechanisms limit swelling: the joint creation of NBO and of O^3, and the formation of Al^5.

The quantities of compensator and modifier Na and Ca were measured before and after irradiation in the initial and final structures relaxed in the NPT and NVE ensembles. The modifiers and compensators were identified as follows. Firstly, all the NBO were noted. These were O with at most one former (Si or Al) in their vicinity. Then for each NBO, the closest Na or Ca was sought. This Na or Ca ion was then considered to be a modifier, because it would stabilize a NBO. By default, all the other Na and Ca were considered to be charge compensators.

Variations in the quantities of modifier Na and Ca under irradiation are indicated in Table 7. Only the modifiers were considered, because the variations in the quantities of compensators are exactly the opposite of those of modifiers, due to the definition adopted.

	Na_{mod}	Ca_{mod}
Na/Ca 1.4	231	-80
Na/Ca 0.3	52	-25
Ca	-	14
Si/Al 5.4	223	-26
Si/Al 2.4	554	64
Si/Al 1.3	511	184

Table 7: Variations in absolute values for Na and Ca in modifiers (Na_{mod} and Ca_{mod}) under irradiation.

The greater the quantity of modifiers formed under irradiation, the weaker the swelling, as shown in Figure 15. The network depolymerisation mechanism leading to the transformation of charge compensators into network modifiers thus constitutes a brake on swelling.

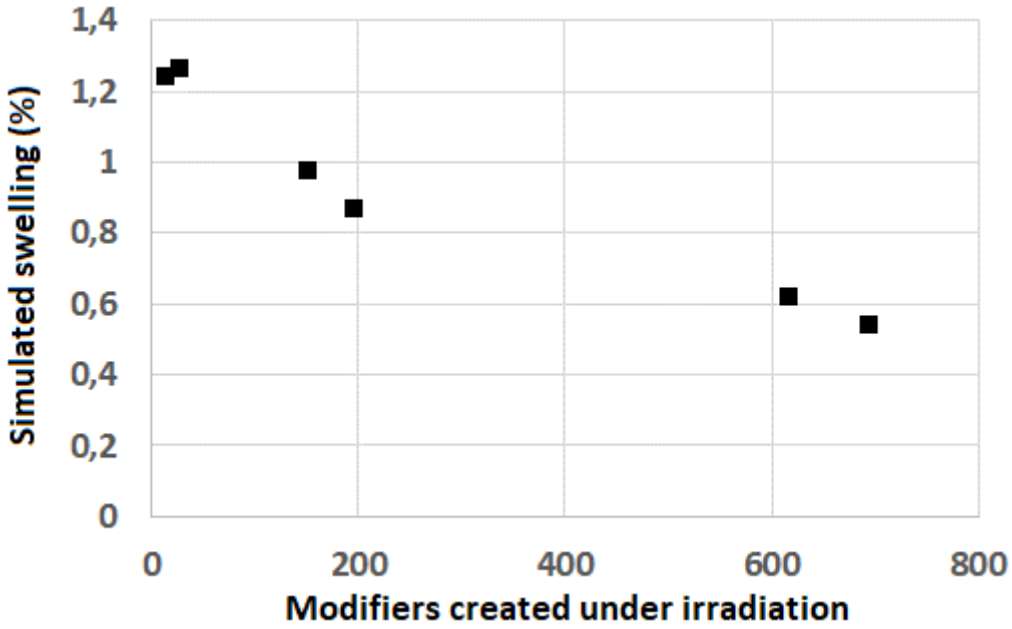

Figure 15: Swelling as a function of the number of modifiers formed under irradiation.

3.4.3 Modification of local volumes

To identify the origin of the density changes more precisely, the local Voronoï volumes around each atom were measured by separating the species according to their coordination and by separating the modifiers and the compensators for the Na and the Ca. Remember that the Voronoï volume of an atom is defined from mediator plans between that atom and its neighbours. It corresponds to all the points closer to that atom than to any other.
The average Voronoï volume values for the different species before and after irradiation are given in Table 8.

Glass	Na/Ca 1.4	Na/Ca 0.3	Ca	Si/Al 5.4	Si/Al 2.4	Si/Al 1.3
Si^4	7.16	7.16	7.17	7.15	7.16	7.16

Si^5	6.97	-	6.61	-	-	-
Al^4	9.40	9.44	9.48	9.38	9.41	9.46
Al^5	8.70	8.98	8.92	8.91	9.01	9.03
NBO	15.14	15.58	15.81	15.11	15.47	15.52
O^2	14.65	14.70	14.72	14.60	14.79	14.79
O^3	12.66	12.79	12.67	13.00	13.02	13.00
Na_m	17.02	17.05	-	17.05	17.46	17.28
Na_c	17.97	18.01	-	17.87	18.30	18.07
Ca_m	15.96	16.10	16.09	16.01	16.46	16.52
Ca_c	16.27	16.54	16.49	16.24	16.68	16.76

Glass	Na/Ca 1.4	Na/Ca 0.3	Ca	Si/Al 5.4	Si/Al 2.4	SiAl 1.3
Si^4	7.20	7.22	7.19	7.19	7.20	7.19
Si^5	6.76	6.73	6.76	6.76	6.67	7.02
Al^4	9.53	9.57	9.50	9.50	9.55	9.58
Al^5	8.89	8.93	8.95	8.93	8.95	8.95
NBO	15.30	15.79	16.07	15.25	15.55	15.65
O^2	14.70	14.83	14.87	14.64	14.84	14.84
O^3	12.79	12.79	12.74	12.90	13.05	13.07
Na_m	17.44	17.44	-	17.38	17.88	17.68
Na_c	18.37	18.58	-	18.35	18.68	18.38
Ca_m	16.44	16.44	16.39	16.44	16.74	16.84
Ca_c	16.71	16.96	16.90	16.77	17.04	16.89

Table 8: Average Voronoï volumes (in $Å^3$) for the different species before (top) and after (bottom) irradiation.

Several results should be noted:
- all the local volumes increased after irradiation, whatever the species considered,
- the highest relative variations concentrate around the Ca, then the Na, then the Al (Table 9 gives the relative variations for the Voronoï volumes),
- the sum of the Voronoï volumes around an O^3 and a NBO is less than twice the Voronoï volume of an O^2,
- the Voronoï volume of an Al^5 is less than that of an Al^4,
- the Voronoï volume around a Na (Ca) modifier is less than that around a Na (Ca) compensator.

Glass	Na/Ca 1.4	Na/Ca 0.3	Ca	Si/Al 5.4	Si/Al 2.4	Si/Al 1.3
Si^4	0.61	0.80	0.57	0.54	0.53	0.43
Si^5	3.11	-	2.16	-	-	-
Al^4	1.38	1.34	1.43	1.31	1.46	1.33
Al^5	2.15	0.51	0.32	0.23	0.71	0.84
NBO	1.05	1.34	1.66	0.96	0.51	0.86
O^2	0.32	0.92	1.01	0.25	0.28	0.32
O^3	1.09	0.00	0.53	0.78	0.23	0.57
Na_m	2.46	2.28	-	1.91	2.43	2.27
Na_c	2.24	3.18	-	2.66	2.06	1.74
Ca_m	3.06	2.16	1.83	2.71	1.71	1.90
Ca_c	2.67	2.55	2.44	3.24	2.18	0.76

Table 9: Relative variations of the Voronoï volumes (in %) around the different species under irradiation.

The correlations previously observed between density variation and structural changes can now be more easily explained in the light of the amplitude of the Voronoï volumes around the different species. It can be seen the fact that the swelling decreases when NBO and O^3 are formed comes from the fact that the sum of the Voronoï volumes around a NBO + O^3 pair is lower than twice the Voronoï volume of an O^2.
The conversions $O^2 + O^2 \rightarrow NBO + O^3$ therefore constitute a first brake on swelling.
Figure 13 also underlines that the formation of Al^5 limited swelling. This correlation is explained simply by the fact that the Voronoï volume of an Al^5 is less than that of an Al^4.

Finally, it was observed that the swelling decreased when the compensators were converted into modifiers (Figure 15). This result is logical if we consider that the Voronoï volume of a modifier (Na or Ca) is less than that of a compensator (Na or Ca).

With this information, a phenomenological model for the density variation under irradiation can be proposed. At the overall scale, the accumulation of displacement cascades causes the vitreous network to "breathe", which means a general increase in all the Voronoï volumes (Table 9). However, this overall phenomenon is locally weighted by structural changes caused by the accumulation of ballistic impacts, i.e. the depolymerisation and the disorganization of the glass (formation of NBO and of O^3 to the detriment of O^2), the conversion of compensators into modifiers, and the formation of Al^5 to the detriment of Al^4. These three local mechanisms constitute brakes on swelling.

The resulting variation in density is then because of the overlapping of several overall and local mechanisms with antagonistic effects. The fact that swelling was systematically observed during the simulations could be explained if the mechanism associated with swelling (vitreous network "breathing") had been overestimated compared to the mechanisms which constitute brakes on swelling. The absence of relaxation in the long term for the glasses after the displacement cascades ended could be the reason. We will return to this point during the discussion.

3.4.4 Quench effect and confirmation of the phenomenological model

To test a different approach to correlating the density changes and structural modifications, and thus to study the question from another angle, glasses with the same compositions as the previous samples were prepared but with the quenching accelerated to 10^{15}K/s instead of 10^{12}K/s. In the same way as for the displacement cascade simulation, the volumes were fixed at the experimental densities to prepare the glasses, and two reference calculations were carried out in the NPT and NVE ensembles with the structures stabilized at 300K in order to estimate the equilibrium volumes for the glasses quenched at 10^{12}K/s and 10^{15}K/s.

Table 10 gives the variations in density under the effect of quench acceleration. Now, depending on the glass composition, quench acceleration can lead to either swelling or shrinkage.

Na/Ca 1.4	Na/Ca 0.3	Ca	Si/Al 5.4	Si/Al 2.4	Si/Al 1.3
0.67	0.97	1.44	0.77	-0.26	-0.27

Table 10: Density variations (in %) between the glasses quenched at 10^{12}K/s and at 10^{15}K/s.

The changes in volume after the quench acceleration correlate fairly well with those caused by irradiation, as shown in Figure 16. The trends are the same, with a difference in the volume changes for the accelerated quench tending towards lower values.

We also sought to correlate the structural changes with the density variations. Table 11 gives the variations in the quantities of the different species following the quench acceleration for each composition.

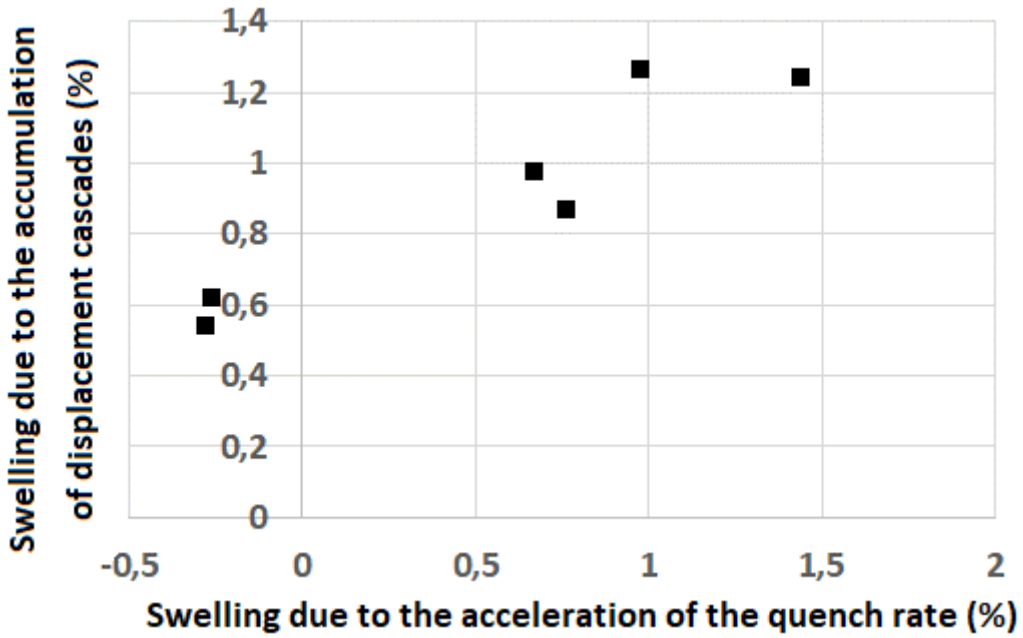

Figure 16: Swelling caused by irradiation as a function of the swelling due to quench acceleration.

Glass	Na/Ca 1.4	Na/Ca 0.3	Ca	Si/Al 5.4	Si/Al 2.4	Si/Al 1.3
Si^5	9	17	18	6	5	4
Al^5	31	25	15	63	171	321
NBO	116	102	171	328	1321	1461
O^3	247	255	305	469	1483	1737
Na_m	63	114	-	106	310	308
Na_c	-63	-114	-	-106	-310	-308
Ca_m	-19	-24	25	-61	-32	129
Ca_c	19	24	-25	61	32	-129

Table 11: Variations in the quantities of the different structural species after quench acceleration.

It is interesting to see that the correlations revealed by the irradiations remain valid under the effect of quench acceleration. The relative variation in volume decreases with the formation of NBO, O^3, Al^5, and of modifiers. In Figure 17, only shows the correlation between the relative variation in volume and the quantity of modifiers created (the correlations between the variation in volume and changes in the quantities of O^3 and of Al^5 are given in the Supplementary Information).

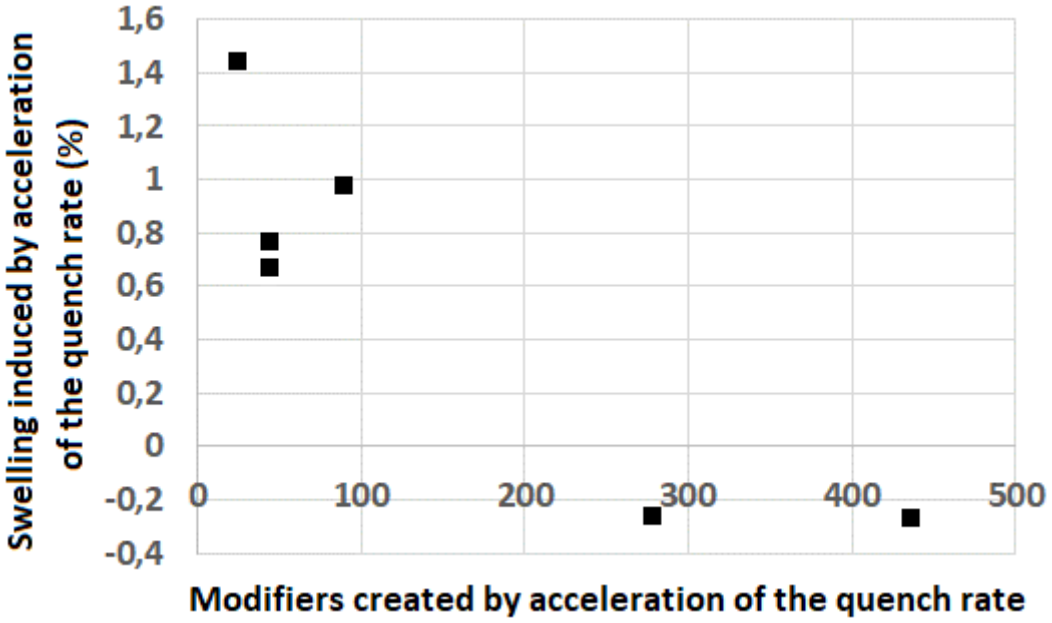

Figure 17: Variation in volume under the effect of quench rate acceleration as a function of the quantity of modifiers created.

Analysis based on the Voronoï volumes enables a better understanding of the differences between the effects of irradiation and those of quenching. Table 12 lists the absolute differences of the Voronoï volumes for the different atomic species following irradiation and those found after quench acceleration.

The most notable differences come from the O and Na environments. The swellings around the O and Na, which were significant under irradiation, became much less obvious under the effect of quench acceleration. Contractions in the O and Na environments could even be observed.
The network "breathing" which has been mentioned above following the accumulation of ballistic impacts is therefore less noticeable when the thermal quench is accelerated and, because of this, the processes that can brake swelling take on a greater role. In the end, certain glasses can even shrink following thermal quench acceleration.

Glass	Na/Ca 1.4	Na/Ca 0.3	Ca	Si/Al 5.4	Si/Al 2.4	Si/Al 1.3
Si	0.044	0.06	0.04	0.04	0.04	0.03
Al	0.14	0.13	0.14	0.13	0.15	0.13
O	0.07	0.15	0.18	0.05	0.02	0.03
Na	0.38	0.45	-	0.37	0.32	0.25
Ca	0.49	0.36	0.31	0.45	0.30	0.19

Glass	Na/Ca 1.4	Na/Ca 0.3	Ca	Si/Al 5.4	Si/Al 2.4	Si/Al 1.3
Si	0.06	0.06	0.06	0.05	0.05	0.05
Al	0.16	0.19	0.18	0.15	0.20	0.18
O	0.02	0.08	0.19	0.02	-0.13	-0.12
Na	0.22	0.26	-	0.32	-0.06	-0.13
Ca	0.71	0.48	0.42	0.69	0.31	0.14

Table 12: Absolute variations in the Voronoï volumes (in $Å^3$) for the different atomic species under irradiation (top) and with the accelerated quench effect (bottom).

Even if the effects of irradiation and of quench acceleration present similarities qualitatively, the intensity of the effects is not the same and can lead to opposite density changes.

4. Discussion

Depending on its composition, a SiO_2-Al_2O_3-Na_2O-CaO glass experimentally irradiated by heavy ions can swell or shrink. By highlighting the motors for and the brakes on swelling, molecular dynamics simulation of displacement cascades and of the effects of quench acceleration in glasses with the same compositions have enabled a better understanding of the origin of the various macroscopic behaviours observed.

A first motor favouring swelling lies in the overall increase seen in all the local volumes around the different atoms under the accumulation of ballistic impacts. This process can be described as a sort of "breathing" of the structure in the core of the displacement cascade. This "breathing" is probably linked to the almost instantaneous quench which follows the thermal peak and which seizes the structure in its current state [37].

Added to this first process are the local environment modifications caused by the ballistic impacts, a process that brakes swelling. The depolymerisation of the network with the conversion of two O^2 into one NBO and one O^3, the conversions of charge compensator Na and Ca into network modifiers, and the formation of Al^5 are the main processes that brake swelling. These processes are even more numerous when the glass initially contains fewer NBO. This explains the correlation observed experimentally between a high initial quantity of NBO and strong swelling.
These different local processes do not occur independently. In fact, the formation of 5-coordinated Al correlates with the formation of O^3, and the conversions of compensators into modifiers are associated with the creation of NBO.

Even if the atomistic modelling enables a better understanding of the competitions between the mechanisms at the origin of density changes, notable differences remain between simulations and experiments, which the authors will now attempt to explain.

The first difference concerns the amplitude of the density variations. During experiments, certain glasses swell under irradiation while others contract, whereas all the glasses swelled during the ballistic effect simulations. This difference may originate from the fact that the relaxation times allowed at the end of the displacement cascades were short (for reasons related to the calculation times), which prevented long-term structural relaxations. These would be likely to suppress part of the free volume generated by the ballistic impacts, and thus an excess of free volume remained which was responsible for an overestimation of the volume changes.
The impossibility of relaxing the irradiated glasses for long periods may also explain the presence of significant quantities of species such as Al^5 or O^3, entities which were not detected in such high quantities by the ^{27}Al NMR (O^3 is very difficult to detect with NMR). The presence of these entities confirms that the structural state at the end of the accumulation of the displacement cascades corresponded to an intermediary state, i.e. not totally relaxed.

The fact that accelerating the quench rate makes it possible to reproduce the experimentally observed swellings and shrinkages is yet another sign that the lack of long-term relaxation in the irradiation simulation prevented the observation of shrinkage phenomena. The quench

effect, however, enabled the reproduction of local structural modifications but without the deposit of free volume that comes from irradiation.

Interestingly, the difference between the simulated and the experimental density changes is even greater when the quantity of SiO_2+Al_2O_3 rises, i.e. when the glass rigidity increases (Figure 18).

Long-term relaxation is even more negatively affected when the glass is rigid, as the structural reorganisations require longer periods. As a result, overestimation of the swelling is more likely for this type of glass as the annealing of the free volume created by ballistic impacts has even less time to occur.

Taken together, these observations - difference between the quench acceleration effects and the ballistic effects, and the increase in the difference between the simulated density change and the experimental data depending on the glass rigidity – have lead us to propose that the impossibility of simulating long relaxation periods at the end of a series of displacement cascades explains why it has not been possible to reproduce the contraction of certain glasses under irradiation.

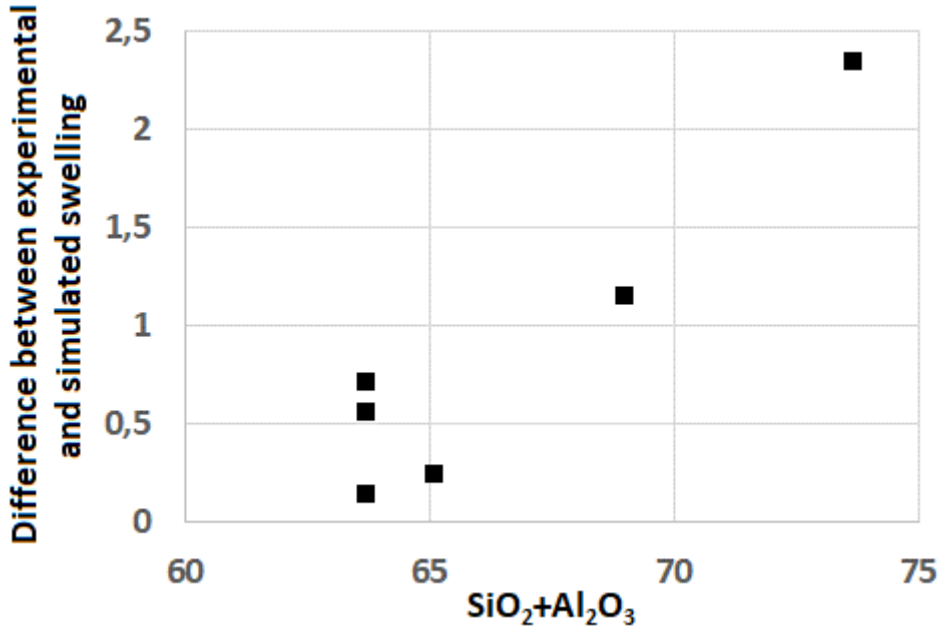

Figure 18: Differences between simulated and experimental swelling as a function of the quantity of SiO_2+Al_2O_3.

Other factors could also have influenced the simulation results, for example simulating irradiation energies which were weaker than the experimental energies, or the relative simplicity of the force fields used and which could not reproduce the entire complexity of the dynamic mechanisms within the glasses.

5. Conclusion

Using molecular dynamics applied to several displacement cascades for six different compositions, and comparing experiments with simulations, has made it possible to propose

an explanation for the origins of density variations in SiO_2-Al_2O_3-Na_2O-CaO glasses under irradiation by heavy ions, sometimes negative, sometimes positive.

The accumulation of ballistic collisions within vitreous structures leads to a deposit of free volumes, linked to the thermal peak in the core of the cascades. This mechanism favours swelling. In parallel, modifications to the local environments caused by irradiation, for example the formation of non-bridging and 3-coordinated oxygens, the formation of 5-coordinated Al, and the conversions between charge compensators and network modifiers, constitute brakes on swelling. The relative involvements of these different mechanisms enable the variability of experimental behaviours to be explained.

The differences found between experimental and simulation results, particularly regarding the amplitude of density changes and their hierarchy among the different compositions, can be explained by a lack of long-term relaxation after the ballistic impact simulations. Such relaxations are inaccessible using our current means of simulation, and this limits the annealing of the free volume accumulated in the core of the cascades. This lack has an even greater effect on simulation when the glass is rigid, i.e. when it contains a high proportion of formers.

Acknowledgements

The authors wish to sincerely thank ORANO, France, EDF, France and the CEA, France, for their financial support during this study.

REFERENCES

[1] S. Gin, A. Abdelouas, L.J. Criscenti, W.L. Ebert, K. Ferrand, T. Geisler, M.T. Harrison, Y. Inagaki, S. Mitsui, K.T. Mueller, J.C. Marra, C.G. Pantano, E.M. Pierce, J.V. Ryan, J.M. Schofield, C.I. Steefel, J.D. Vienna, Mater. Today, 16 (2013) 243-248.
[2] W.J. Weber, R.C. Ewing, C.A. Angell, G.W. Arnold, A.N. Cormack, J.M. Delaye, D.L. Griscom, L.W. Hobbs, A. Navrotsky, D.L. Price, A.M. Stoneham, M.C. Weinberg, J. Mater. Res. 12 (1997) 1946–1978.
[3] S. Peuget, J.-M. Delaye, C. Jégou, J. Nucl. Mater. 444 (2014) 76–91.
[4] J.-M. Delaye, D. Ghaleb, Phys. Rev. B 61 (2000) 14481–14494.
[5] W.J. Weber, Procedia Mater. Sci. 7 (2014) 237–246.
[6] P. Chevreux, A. Laplace, E. Deloule, I. Tissandier, N. Massoni, J. Non-Cryst. Solids, 457 (2017) 13-24.
[7] D.R. Neuville, L. Cormier, B. Boizot, A.-M. Flank, J. Non. Cryst. Solids 323 (2003) 207–213.
[8] K. Chah, B. Boizot, B. Reynard, D. Ghaleb, G. Petite, Nucl. Instruments Methods Phys. Res. Sect. B. 191 (2002) 337–341.
[9] L. Cormier, D.R. Neuville, Chem. Geol., 213 (2004) 103-113.
[10] D.R. Neuville, L. Cormier, A.-M. Flank, V. Briois, D. Massiot, Chem. Geol., 213 (2004) 153-163.
[11] A. Le Gac, B. Boizot, C. Jégou, S. Peuget, Nucl. Instruments Methods Phys. Res. Sect. B. 407 (2017) 203-209.
[12] J.-M. Delaye, S. Peuget, G. Bureau, G. Calas, J. Non-Cryst. Solids, 357 (2011) 2763-2768.
[13] J.-M. Delaye, D. Ghaleb, Phys. Rev. B 71 (2005) 224204.
[14] D.A. Kilymis, J.-M. Delaye, S. Ispas, J. Chem. Phys. 145 (2016) 44505.
[15] L.H. Kieu, J.-M. Delaye, C. Stolz, J. Non-Cryst. Solids, 358 (2012) 3268-3279.
[16] N.M.A. Krishnan, Y. Le Pape, G. Sant, M. Bauchy, J. Nucl. Mater., 512 (2018) 126-136.
[17] L. Deng, J. Du, J. Am. Ceram. Soc., 102 (2018) 2482-2505.
[18] S. Sundararaman, L. Huang, S. Ispas, W. Kob, J. Chem. Phys., 150 (2019) 154505.
[19] B. Guillot, N. Sator, Geochim. Cosmochim. Acta, 71 (2007) 1249-1265.
[20] M.T. Ha, S.H. Garofalini, J. Am. Ceram. Soc., 100 (2017) 563-573.
[21] M.Y. Wang, N.M.A. Krishnan, B. Wang, M.M. Smedskjaer, J.C. Mauro, M. Bauchy, J. Non-Cryst. Solids, 498 (2018) 294-304.
[22] F. Lodesani, M.C. Menziani, H. Hijiya, Y. Takato, S. Urata, A. Pedone, Sci. Rep., 10 (2020) 2906.

[23] A. Jan, J.-M. Delaye, S. Gin, S. Kerisit, J. Non-Cryst. Solids, 505 (2019) 188-201.
[24] J.-M. Delaye, A. Le Gac, S. Macaluso, F. Angeli, T. Charpentier, S. Peuget, submitted.
[25] A.H. Mir, S. Peuget, M. Toulemonde, P. Bulot, C. Jegou, S. Miro, S. Bouffard, Europhysics Lett., 112 (2015) 36002.
[26] A.H. Mir, PhD « Radiation effects on oxide glasses: Importance of energy deposition and relaxation processes. », Université de Caen, 2015.
[27] A. LeGac, PhD « Comportement sous irradiation des verres d'alumino silicates », Université Paris – Saclay, 2017.
[28] S. W. De Leeuw, J. W. Perram, E. R. Smith, Proc. Roy. Soc. London 373 (1980) 27-56.
[29] S. W. De Leeuw, J. W. Perram, E. R. Smith, Proc. Roy. Soc. London 373 (1980) 57-66.
[30] I.T. Todorov, W. Smith, K. Trachenko, M.T. Dove, J. Mater. Chem., 16 (2006) 1911.
[31] J.B. Ziegler, J.P. Biersack, U. Littmark, The stopping power and ranges of ions in matter, (1985).
[32] P. McMillan, B. Piriou, J. Non-Cryst. Solids, 53 (1982) 279-298.
[33] D. Neuville, L. Cormier, D. Massiot, Geochim. Cosmochim. Acta, 68 (2004) 5071-5079.
[34] N. Trcera, S. Rossano, M. Tarrida, J. Raman Spectrosc., 42 (2011) 765-772.
[35] J.A.C. Marples, Nucl. Instr. Meth. B, 32 (1988) 480.
[36] D.A. Kilymis, J.-M. Delaye, S. Ispas, J. Non-Cryst. Solids, 432 (2016) 354.
[37] S. Peuget, E.A. Maugeri, T. Charpentier, C. Mendoza, M. Moskura, T. Fares, O. Bouty, C. Jegou, J. Non-Cryst. Solids, 378 (2013) 201-212.